Making trotters sprint: A variational imaginary time ansatz for quantum many-body systems

Matthew J. S. Beach,[1,2] Roger G. Melko,[1,2] Tarun Grover,[3] and Timothy H. Hsieh[1]
[1]*Perimeter Institute for Theoretical Physics, Waterloo, Ontario, Canada N2L 2Y5*
[2]*Department of Physics and Astronomy, University of Waterloo, Waterloo, Ontario, Canada N2L 3G1*
[3]*Department of Physics, University of California at San Diego, La Jolla, California 92093, USA*

(Received 10 April 2019; revised manuscript received 25 July 2019; published 20 September 2019)

We introduce a variational wave function for many-body ground states that involves imaginary-time evolution with two different Hamiltonians in an alternating fashion with variable time intervals. We successfully apply the ansatz on the one- and two-dimensional transverse-field Ising model and systematically study its scaling for the one-dimensional model at criticality. We find the total imaginary time required scales logarithmically with system size, in contrast to the linear scaling in conventional quantum Monte Carlo. We suggest this is due to unique dynamics permitted by alternating imaginary-time evolution, including exponential growth of bipartite entanglement. For generic models, the superior scaling of our ansatz potentially mitigates the negative sign problem at the expense of having to optimize variational parameters.

DOI: 10.1103/PhysRevB.100.094434

I. INTRODUCTION

Imaginary time plays a prominent role in multiple branches of physics, including cosmology, statistical mechanics, and quantum field theory. The seemingly simple replacement of real time, t, with its imaginary counterpart, $\tau = -it$, leads to fundamental connections between quantum theory and statistical mechanics [1]. Such connections enable the efficient simulation of many quantum systems using quantum Monte Carlo techniques [2–4]. However, for many physically interesting models, these methods suffer from the prohibitive "negative sign problem" [5,6], which requires an exponential amount of computational resources to obtain reasonable accuracy for quantum many-body systems. Many outstanding problems in condensed matter, such as those involving high-temperature superconductors or topologically ordered phases, require an understanding of complex interacting models which are unsolved with present techniques.

One class of Monte Carlo methods that can avoid the sign problem are so-called variational Monte Carlo (VMC) methods [7–11]. In VMC, one assumes a sufficiently general trial state that depends on adjustable parameters. These parameters are then chosen to minimize the energy with respect to the given Hamiltonian. Finding an effective trial state such as Jastrow [11], matrix product states [12–14], or neural network states [15–18], can result in efficient simulation of interacting quantum systems. The key to the success of these techniques is a well-chosen ansatz that reflects the properties of the target phase and the existence of a viable optimization scheme [19,20].

The recent advent of quantum computers and simulators has motivated the development of new variational approaches [21]. Such variational quantum algorithms involve applying a sequence of unitary operators, parametrized by several variables onto a easy-to-prepare initial state. The variables are chosen to optimize a given cost function involving the resulting wave function. For example, in the quantum approximate optimization algorithm (QAOA) [22–26] the cost function is a classical Hamiltonian encoding a combinatorial optimization problem, and the variational wave function is prepared by alternating between evolving with the Hamiltonian and a transverse field. The evolution times constitute variational parameters that are optimized to minimize the Hamiltonian cost function. This variational approach has been generalized for preparing both strongly correlated and highly entangled states on near-term quantum devices [27–29].

Motivated by the success of such variational approaches, in this paper we propose a variational ansatz for ground states of quantum many-body systems which involves sequentially evolving with different Hamiltonians in imaginary time. In contrast to real-time evolution with local Hamiltonians, which is limited by Lieb-Robinson bounds on the growth of correlation functions, imaginary-time evolution does not have this constraint and can exhibit remarkable efficiency in traversing Hilbert space.

As proof of concept, we demonstrate the efficiency of our ansatz in representing the ground state of the transverse-field Ising model at criticality. Whereas standard projector methods require imaginary-time scaling with system size L to reach the critical ground state, we show numerically that our ansatz requires time scaling logarithmically with L. Furthermore, we analyze how entanglement grows after each imaginary-time operation in our ansatz, and we find an exponential growth that is a unique feature of imaginary-time dynamics. We conclude by demonstrating that the ansatz continues to perform well in the presence of integrability-breaking perturbations, and we mention generalizations of our ansatz to other models, including those with sign problems. We envision the main purpose of this ansatz to be an efficient trial wave function for quantum many-body physics on (classical) computers; however, it is possible that one can also implement such imaginary-time evolution natively on a quantum computer [30,31].

II. ANSATZ

Many Hamiltonians are naturally a linear combination of two components $H = H_A + gH_B$, where $H_{A,B}$ are individually tractable to analyze. Examples include transverse-field Ising, Hubbard, and the J_1-J_2 model. Motivated by the QAOA procedure, we consider the following variational imaginary-time ansatz (VITA) for the ground state of H:

$$|\psi_P(\boldsymbol{\alpha}, \boldsymbol{\beta})\rangle = \mathcal{N} e^{-\beta_P H_B} e^{-\alpha_P H_A} \cdots e^{-\beta_1 H_B} e^{-\alpha_1 H_A} |\psi_0\rangle, \quad (1)$$

where P is the number of pairs of variational parameters $\boldsymbol{\alpha} = (\alpha_1, \ldots, \alpha_P)$, $\boldsymbol{\beta} = (\beta_1, \ldots, \beta_P)$, $|\psi_0\rangle$ is an initial state, and $\mathcal{N}$ is a normalization factor. We further define the total imaginary time $\tau = \frac{1}{2}\sum_{p=1}^{P}(\alpha_p + \beta_p)$. A circuit representation is shown in Fig. 1. The bang-bang, or square-pulse, style of the ansatz is optimal for quantum control in real-time QAOA as per Pontryagin's principle [32].

While VITA is applicable to any Hamiltonian, in specific cases there is explicit physical motivation for considering such an ansatz. For example, for the fermionic Hubbard model, the $P = 1$ ansatz reduces to Otsuka's generalization of the Gutzwiller variational wave function [7,9,10], which seeks to balance single occupancy per site with itinerancy. The $P \leqslant 3$ case has been considered in Ref. [33] for the two-dimensional Hubbard model, but a systematic analysis of how its performance scales with system size and P was not carried out. A related variational approach for the Hubbard model has also been considered in Ref. [34].

The standard projector method for attaining the ground state of H involves evaluating $e^{-\tau H}|\psi_0\rangle$ for $\tau \gtrsim 1/\Delta$ where Δ is the many-body spectral gap. This can be decomposed via Trotterization into a sequence of the VITA form, with parameters $\alpha_p = \beta_p = \tau/2P$ for large P. This guarantees that VITA can exactly represent the ground state in the $P \to \infty$ limit. However, the projector method is especially expensive for critical systems where $\Delta \sim 1/L$, and hence τ scales polynomially with L. One can consider Eq. (1) as a nonuniform Trotterization with large (and variable) time steps. We will show that remarkably high fidelities can be attained even with τ that is *exponentially smaller* compared to the aforementioned estimate from the standard projector method.

We first present some general considerations of why such an ansatz may be efficient. It is useful to first compare with

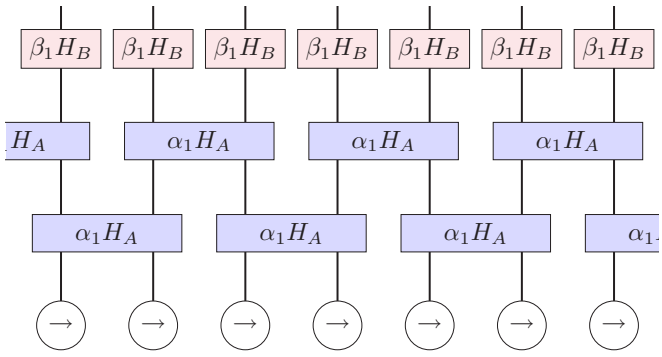

FIG. 1. Circuit representation of the trial state $|\psi_P(\boldsymbol{\alpha}, \boldsymbol{\beta})\rangle$ for $P = 1$. Each box denotes imaginary-time evolution with the enclosed Hamiltonian.

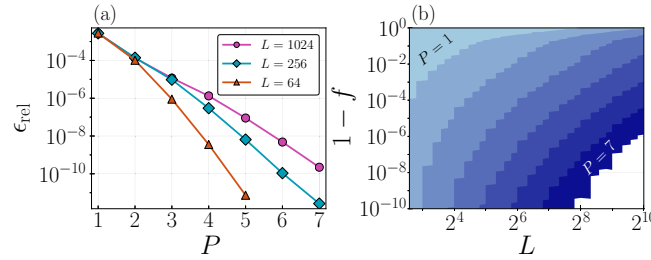

FIG. 2. (a) Relative error in energy, $\epsilon_{\rm rel}$, between the exact ground state energy, $E_{\rm exact}$, and the energy of the optimized trial wave function $E_P(\boldsymbol{\alpha}, \boldsymbol{\beta})$. (b) Number of pulses P needed to obtain a desired accuracy in the fidelity, f, for a given system size, L. The white region was not computed in the present study.

the real-time analog, which are QAOA-type circuits involving alternating real-time evolution between two Hamiltonians. The Lieb-Robinson bound dictates that real-time evolution with local Hamiltonians can generate correlations only within a light cone, and thus there are lower bounds on the time it takes to prepare highly correlated states starting from unentangled product states. For example, in one dimension, the total time to prepare the Greenberger-Horne-Zeilinger (GHZ; "cat") state $\frac{1}{\sqrt{2}}(|11\cdots1\rangle + |00\cdots0\rangle)$ scales at least linearly with system size L [28,35]. In contrast, by evolving with the GHZ parent Hamiltonian $H_{ZZ} = -\sum_{i=1}^{L} Z_i Z_{i+1}$ in imaginary time (Z is the Pauli-Z matrix), the GHZ state can be prepared with imaginary-time scaling as $\log L$ [36].

III. APPLICATION

We test VITA on the transverse-field Ising model (TFIM)

$$H = H_{ZZ} + hH_X \equiv -\sum_{i=1}^{N} Z_i Z_{i+1} - h\sum_{i=1}^{N} X_i \quad (2)$$

with periodic boundary conditions on a system with N spins. Z, X are the Pauli matrices, and h is the transverse-field strength. Our ansatz in this case starts from the paramagnetic ground state of H_X, $|+\rangle$, and alternates between $H_A = H_{ZZ}$ and $H_B = H_X$.

The Ising chain can be mapped to free fermions via the Jordan-Wigner transformation [37] which allows for the efficient evaluation of Eq. (1). We can thus optimize our ansatz for very large system sizes and several pulses. This allows us to properly characterize how efficient the VITA ansatz is without introducing sampling error. For a fixed P, optimization involves finding the minima of the energy cost function $E_P(\boldsymbol{\alpha}, \boldsymbol{\beta}) = \langle\psi_P(\boldsymbol{\alpha}, \boldsymbol{\beta})|H|\psi_P(\boldsymbol{\alpha}, \boldsymbol{\beta})\rangle$.

We first focus on approximating the critical ground state of H at $h = 1$. Figure 2(a) shows the relative error in energy $\epsilon_{\rm rel} = |(E_P(\boldsymbol{\alpha}, \boldsymbol{\beta}) - E_{\rm exact})/E_{\rm exact}|$ where $E_{\rm exact}$ is the exact ground state energy at the critical point, for various P. Evidently, increasing P dramatically improves the accuracy in the energy, even for large system sizes. Optimized parameters for various P are provided in the Supplemental Material [38].

Since the exact ground state for the TFIM is known, we also compare the fidelity, f, of the optimized trial state with the target state. The error in fidelity, $1 - f \equiv 1 -$

$|\langle\psi_{\text{exact}}|\psi_P(\boldsymbol{\alpha}, \boldsymbol{\beta})\rangle|^2$, is shown in Fig. 2(b) for various P, L. The efficiency is quite remarkable; for example, for $L = 64, P = 2$ is already sufficient to approximate the critical state to within around 10^{-4} in relative energy and 10^{-2} in fidelity. Recall that the error in fidelity provides an upper bound for the error in any observable [38].

IV. ENTANGLEMENT DYNAMICS

While there is no Lieb-Robinson bound limiting the rate for generating long-range correlations in our ansatz, entanglement considerations provide lower bounds on the iterations P required to prepare the critical state. Ignoring normalization, imaginary-time evolution with a local Hamiltonian can be represented by a (nonunitary) quantum circuit; each iteration of our ansatz corresponds to three layers shown in Fig. 1. After P pulses, the bipartite entanglement entropy between the left and right halves of the system, hereafter abbreviated EE, can be attained by bisecting the circuit through P bonds. Hence, EE after P iterations is at most $P \log D$, where D is the Schmidt rank (number of singular values) upon decomposing a single two-qubit imaginary-time operator.

In order to generate the EE of the critical state, which scales as $S \propto \log L$, we need the number of pulses scaling at least as $P \propto \log L$. We observe that Fig. 2(b) is consistent with this scaling form. For example, for a target fidelity error of 10^{-10}, each additional P in the ansatz can represent a system approximately twice as large.

The entanglement dynamics in imaginary-time evolution can be considerably different from its real-time counterpart. For real-time evolution, EE across a bipartition can increase only by acting with an operator supported on both sides of the partition. If the circuit in Fig. 1 were unitary, any increase in EE from one layer to the next would be bounded by a constant depending on the two-qubit unitary but not on the state being acted on (see the "small incremental entangling theorem" [39]). In contrast, even imaginary-time operators acting on one side of the bipartition can generate entanglement across the cut. As a very simple example involving two spins, the action of $e^{-\beta Z_1}$ on $\eta_+|11\rangle + \eta_-|00\rangle$ can increase EE as long as $|\eta_+| > |\eta_-| > 0$. This illustrates that the more entangled the initial state, the more imaginary-time evolution can change the entanglement. The change is not simply bounded by a state-independent constant. This allows in principle an exponential growth of EE, as long as the total EE after P steps lies below $P \log D$.

Our ansatz exhibits such dynamics. We take the $P = 5$ ansatz and analyze the EE of the states at intermediate steps, p, of our protocol using the technique of [40,41]. We find that the EE increases exponentially with imaginary time [Fig. 3(a)]. Moreover, for every intermediate state, we plot the mutual information $(S_A + S_B - S_{AB})$ between two spins A, B as a function of their separation [Fig. 3(b)]. The power-law decay for every step is in stark contrast to any local real-time evolution and illustrates the ability of imaginary-time evolution to generate long-range correlations [42]. We find that under imaginary-time evolution, entanglement starts to grow immediately following a local quench, in contrast to real-time evolution [43] where it takes a time proportional to ℓ before growing, ℓ being the distance between the location of the local quench and the entanglement cut.

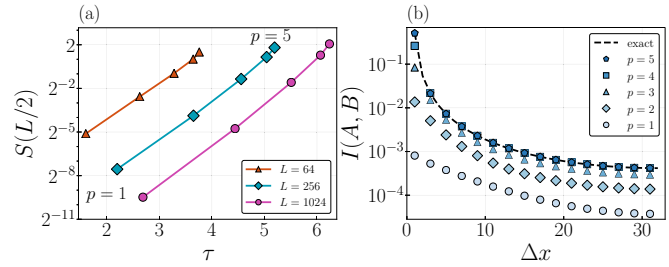

FIG. 3. (a) Entanglement entropy of half partition grows exponentially with imaginary time τ, in the optimal $P = 5$ ansatz for the critical state. (b) Mutual information between two spins at positions A and B, respectively, as a function of their distance Δx, for intermediate steps p in the $P = 5$ protocol with $L = 64$.

V. SCALING

To compare directly with the projector method, we also investigate the total imaginary time $\tau \equiv \frac{1}{2}\sum_{p=1}^{P}(\alpha_p + \beta_p)$ required to achieve a target fidelity. Motivated by the $P \propto \log L$ scaling for achieving a target fidelity, we propose a scaling form of $1 - f = G[\tau(\log L)^{-\nu}]$ for some exponent ν. In Fig. 4, we perform a scaling collapse for $L \in [4, 6, \ldots, 1024]$, and $P \in [1, \ldots, 7]$ and find the optimal exponent $\nu = 2.3 \pm 0.1$. This logarithmic scaling is an exponential speedup compared to the linear scaling of the projector method, $1 - f = F(\tau L^{-1})$ [44].

VI. MONTE CARLO APPROACH

While the TFIM model admits a dual representation as free fermions, for a general model sampling methods are crucial for estimating the energy cost function. As a proof of concept, we also use Monte Carlo sampling for stochastically optimizing VITA.

The quantum-classical correspondence maps quantum observables to dual classical observables of a classical anisotropic Ising model on an $L \times (2P + 1)$ lattice. We denote the classical spin configurations by $\{s\}$ and the spatial and imaginary time by (i, p), respectively [45].

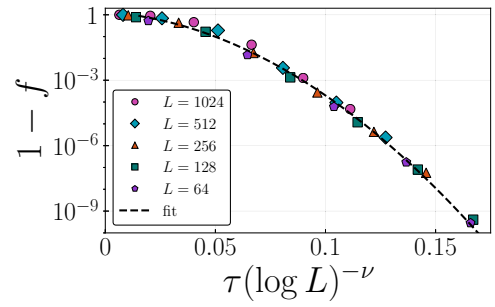

FIG. 4. Collapse of the infidelity $\log(1 - f) = G(\frac{\tau}{(\log L)^{\nu}})$ with $\nu = 2.3$. The fit is a power law $\log(1 - f) = 175x^{1.85}$ with $x = \frac{\tau}{(\log L)^{\nu}}$.

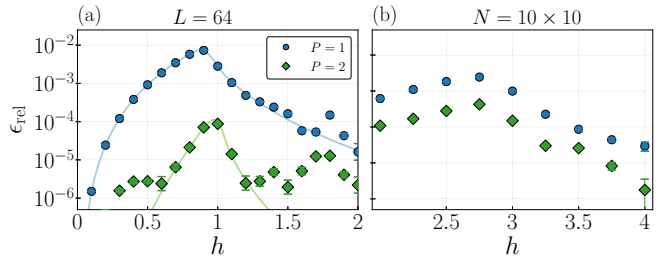

FIG. 5. Relative error in energy, $\epsilon_{\rm rel}$, for VMC using our ansatz on the TFIM: (a) one-dimensional model with $L = 64$ spins. Solid lines denote the results from the free fermion approach. (b) Two-dimensional model on a 10×10 square lattice. Energies are compared with those from zero-temperature stochastic series expansion [47].

The expectation value of a quantum observable $\mathcal{O}$ is

$$\langle \psi_P(\boldsymbol{\alpha}, \boldsymbol{\beta}) | \mathcal{O} | \psi_P(\boldsymbol{\alpha}, \boldsymbol{\beta}) \rangle = \sum_{\{s\}} \tilde{\mathcal{O}}(s)\, p_{\boldsymbol{\alpha},\boldsymbol{\beta}}(s), \tag{3}$$

where $\tilde{\mathcal{O}}$ are dual classical observables, and $p_{\boldsymbol{\alpha},\boldsymbol{\beta}}(s)$ is the Boltzmann weight corresponding to the Ising model with couplings $J_x(p) = \alpha_p, J_\tau(p) = \frac{1}{2} \ln \coth \beta_p$ between nearest neighbors in space and imaginary time, respectively. The couplings vary with imaginary time, p, but are uniform in space. In this way, the energy of the trial wave function can be sampled efficiently with Monte Carlo.

We use this scheme with $P = 1, 2$ to target the ground states for various values of the transverse field h in both the (integrable) one-dimensional and the (nonintegrable) two-dimensional TFIM. We use stochastic natural gradient descent (stochastic reconfiguration) to optimize the parameters [20]. We find rapid convergence for $P = 1$, while higher P becomes more difficult, especially for with a noisy objective function.

The relative error in energy achieved is shown in Fig. 5, with the free fermion results for comparison. For $P = 1$ the VMC achieves the same accuracy as the free fermion method. However, for $P = 2$ away from the critical point $h = 1$, the VMC performance is limited by sampling error [46].

VII. DISCUSSION

We have introduced a variational technique that is motivated by both projector methods and recently developed quantum algorithms. It provides substantial shortcuts to the usual Trotterization of imaginary-time evolution, at the expense of making the procedure variational. Using TFIM as a first testbed, we have demonstrated that this ansatz is viable for sampling methods and highly efficient. In particular, the number of variational parameters required to represent the TFIM critical state scales as $\sim \log L$, in contrast to other variational methods such as density matrix renormalization group, which in this critical case requires bond dimension scaling with L and thus the number of parameters scaling with L^2. One reason for this efficiency is the fact that imaginary-time evolution is not subject to many bounds for real-time evolution; despite being generated by local Hamiltonians, our ansatz exhibits an exponential growth of entanglement entropy and rapid generation of long-range correlations, features unique to imaginary-time evolution.

Our variational approach is potentially useful in the many situations where imaginary-time Trotterization involves a prohibitively large number of steps. For example, in models with a sign problem, the computational cost scales exponentially with space and imaginary time $\mathcal{O}(\tau L^d)$. Our ansatz provides a variational shortcut that significantly reduces τ [from $\tau \sim L$ to $\tau \sim (\log L)^{2.3}$ in the critical one-dimensional TFIM] which could enable the study of larger systems even with a sign problem. For few variational parameters ($P = 1, 2$), the optimization may be feasible, and we leave these investigations to future work.

ACKNOWLEDGMENTS

The authors would like to thank J. Carrasquilla, L. E. Hayward Sierens, E. Inack, and B. Kulchytskyy for many useful discussions. This research was supported by the Natural Sciences and Engineering Research Council of Canada (NSERC), the Canada Research Chair program, and the Perimeter Institute for Theoretical Physics. This work was made possible by the facilities of the Shared Hierarchical Academic Research Computing Network (SHARCNET) and Compute/Calcul Canada. Research at Perimeter Institute is supported by the Government of Canada through Industry Canada and by the Province of Ontario through the Ministry of Research and Innovation. T.G. is supported by the National Science Foundation under Grant No. DMR-1752417, and through an Alfred P. Sloan Research fellowship. This research was supported in part by the National Science Foundation under Grant No. NSF PHY-1748958.

[1] G. C. Wick, Properties of Bethe-Salpeter Wave Functions, Phys. Rev. **96**, 1124 (1954).

[2] D. C. Handscomb, The Monte Carlo method in quantum statistical mechanics, Math. Proc. Cambridge Philos. Soc. **58**, 594 (1962).

[3] R. Blankenbecler and R. L. Sugar, Projector Monte Carlo method, Phys. Rev. D **27**, 1304 (1983).

[4] Anders W. Sandvik and Juhani Kurkijärvi, Quantum Monte Carlo simulation method for spin systems, Phys. Rev. B **43**, 5950 (1991).

[5] E. Y. Loh, J. E. Gubernatis, R. T. Scalettar, S. R. White, D. J. Scalapino, and R. L. Sugar, Sign problem in the numerical simulation of many-electron systems, Phys. Rev. B **41**, 9301 (1990).

[6] M. Troyer and U.-J. Wiese, Computational Complexity and Fundamental Limitations to Fermionic Quantum Monte Carlo Simulations, Phys. Rev. Lett. **94**, 170201 (2005).

[7] Martin C. Gutzwiller, Effect of Correlation on the Ferromagnetism of Transition Metals, Phys. Rev. Lett. **10**, 159 (1963); Correlation of Electrons in a Narrow *s* Band, Phys. Rev. **137**, A1726 (1965).

[8] D. Ceperley, G. V. Chester, and M. H. Kalos, Monte Carlo simulation of a many-fermion study, Phys. Rev. B **16**, 3081 (1977).

[9] H. Otsuka, Variational Monte Carlo Studies of the Hubbard model in one- and two-Dimensions—Off-diagonal intersite correlation effects, J. Phys. Soc. Jpn. **61**, 1645 (1992).

[10] D. Baeriswyl, Variational schemes for many-electron systems, in *Nonlinearity in Condensed Matter*, Springer Series in Solid-State Sciences, edited by Alan R. Bishop, David K. Campbell, Pradeep Kumar, and Steven E. Trullinger (Springer, Berlin/Heidelberg, 1987), pp. 183–193.

[11] F. Becca and S. Sorella, *Quantum Monte Carlo Approaches for Correlated Systems*, 1st ed. (Cambridge University Press, Cambridge, United Kingdom/New York, NY, 2017).

[12] F. Verstraete, D. Porras, and J. I. Cirac, Density Matrix Renormalization Group and Periodic Boundary Conditions: A Quantum Information Perspective, Phys. Rev. Lett. **93**, 227205 (2004).

[13] A. W. Sandvik and G. Vidal, Variational Quantum Monte Carlo Simulations with Tensor-Network States, Phys. Rev. Lett. **99**, 220602 (2007).

[14] G. Vidal, Classical Simulation of Infinite-Size Quantum Lattice Systems in One Spatial Dimension, Phys. Rev. Lett. **98**, 070201 (2007).

[15] G. Carleo and M. Troyer, Solving the quantum many-body problem with artificial neural networks, Science **355**, 602 (2017).

[16] N. Freitas, G. Morigi, and V. Dunjko, Neural network operations and Susuki–Trotter evolution of neural network states, Int. J. Quantum. Inf. **16**, 1840008 (2018).

[17] E. M. Inack, G. E. Santoro, L. Dell'Anna, and S. Pilati, Projective quantum Monte Carlo simulations guided by unrestricted neural network states, Phys. Rev. B **98**, 235145 (2018).

[18] S. Pilati, E. M. Inack, and P. Pieri, Self-learning projective quantum Monte Carlo simulations guided by restricted Boltzmann machines, arXiv:1907.00907.

[19] C. J. Umrigar, K. G. Wilson, and J. W. Wilkins, Optimized Trial Wave Functions for Quantum Monte Carlo Calculations, Phys. Rev. Lett. **60**, 1719 (1988).

[20] S. Sorella, Green Function Monte Carlo with Stochastic Reconfiguration, Phys. Rev. Lett. **80**, 4558 (1998); Generalized Lanczos algorithm for variational quantum Monte Carlo, Phys. Rev. B **64**, 024512 (2001); Wave function optimization in the variational Monte Carlo method, *ibid.* **71**, 241103(R) (2005).

[21] Tyson Jones, Suguru Endo, Sam McArdle, Xiao Yuan, and Simon C. Benjamin, Variational quantum algorithms for discovering Hamiltonian spectra, Phys. Rev. A **99**, 062304 (2019).

[22] E. Farhi, J. Goldstone, and S. Gutmann, A quantum approximate optimization algorithm, arXiv:1411.4028.

[23] L. Zhou, S.-T. Wang, S. Choi, H. Pichler, and M. D. Lukin, Quantum approximate optimization algorithm: Performance, mechanism, and implementation on near-term devices, arXiv:1812.01041.

[24] Z. Wang, S. Hadfield, Z. Jiang, and E. G. Rieffel, Quantum approximate optimization algorithm for MaxCut: A fermionic view, Phys. Rev. A **97**, 022304 (2018).

[25] S. Hadfield, Z. Wang, B. O'Gorman, E. G. Rieffel, D. Venturelli, and R. Biswas, From the quantum approximate optimization algorithm to a quantum alternating operator ansatz, Algorithms **12**, 34 (2019).

[26] G. Verdon, J. M. Arrazola, K. Brádler, and N. Killoran, A quantum approximate optimization algorithm for continuous problems, arXiv:1902.00409.

[27] D. Wecker, M. B. Hastings, and M. Troyer, Progress towards practical quantum variational algorithms, Phys. Rev. A **92**, 042303 (2015).

[28] W. W. Ho and T. H. Hsieh, Efficient variational simulation of non-trivial quantum states, SciPost Phys. **6**, 029 (2019).

[29] W. W. Ho, C. Jonay, and T. H. Hsieh, Ultrafast variational simulation of nontrivial quantum states with long-range interactions, Phys. Rev. A **99**, 052332 (2019).

[30] S. McArdle, T. Jones, S. Endo, Y. Li, S. Benjamin, and X. Yuan, Variational quantum simulation of imaginary time evolution, arXiv:1804.03023.

[31] M. Motta, C. Sun, A. T. K. Tan, M. J. O'Rourke, E. Ye, A. J. Minnich, F. G. S. L. Brandao, and G. K.-L. Chan, Quantum imaginary time evolution, quantum Lanczos, and quantum thermal averaging, arXiv:1901.07653.

[32] Z.-C. Yang, A. Rahmani, A. Shabani, H. Neven, and C. Chamon, Optimizing Variational Quantum Algorithms Using Pontryagin's Minimum Principle, Phys. Rev. X **7**, 021027 (2017).

[33] T. Yanagisawa, S. Koike, and K. Yamaji, Off-diagonal wave function Monte Carlo studies of Hubbard model I, J. Phys. Soc. Jpn. **67**, 3867 (1998); T. Yanagisawa, Crossover from weakly to strongly correlated regions in the two-dimensional Hubbard model—Off-diagonal wave function Monte Carlo studies of Hubbard model II, *ibid.* **85**, 114707 (2016); Antiferromagnetism, superconductivity and phase diagram in the two-dimensional Hubbard model—Off-diagonal wave function Monte Carlo studies of Hubbard model III, *ibid.* **88**, 054702 (2019).

[34] M.-S. Vaezi and A. Vaezi, A unified theory of variational and quantum Monte Carlo methods and beyond, arXiv:1810.00864.

[35] S. Bravyi, M. B. Hastings, and F. Verstraete, Lieb-Robinson Bounds and the Generation of Correlations and Topological Quantum Order, Phys. Rev. Lett. **97**, 050401 (2006).

[36] See Supplemental Material at http://link.aps.org/supplemental/10.1103/PhysRevB.100.094434 for a short proof that τ scales as $\log L$ for the GHZ state preparation.

[37] E. Lieb, T. Schultz, and D. Mattis, Two soluble models of an antiferromagnetic chain, Ann. Phys. (NY) **16**, 407 (1961).

[38] See Supplemental Material at http://link.aps.org/supplemental/10.1103/PhysRevB.100.094434 for the optimal parameters dependence on L and P.

[39] M. Mariën, K. M. R. Audenaert, K. Van Acoleyen, and F. Verstraete, Entanglement rates and the stability of the area law for the entanglement entropy, arXiv:1411.0680.

[40] I. Peschel, Calculation of reduced density matrices from correlation functions, J. Phys. A: Math. Gen. **36**, L205 (2003).

[41] G. Vidal, J. I. Latorre, E. Rico, and A. Kitaev, Entanglement in Quantum Critical Phenomena, Phys. Rev. Lett. **90**, 227902 (2003); J. I. Latorre, E. Rico, and G. Vidal, Ground state entanglement in quantum spin chains, Quantum Inf. Comput. **4**, 48 (2004).

[42] See Supplemental Material at http://link.aps.org/supplemental/10.1103/PhysRevB.100.094434 for considerations of a local quench in imaginary time in a conformal field theory.

[43] P. Calabrese and J. Cardy, Evolution of entanglement entropy in one-dimensional systems, J. Stat. Mech.: Theory Exp. (2005) P04010; Entanglement and correlation functions following a

local quench: A conformal field theory approach, *ibid.* (2007) P10004.

[44] L. Liu, A. W. Sandvik, and W. Guo, Typicality at quantum-critical points, Chin. Phys. B **27**, 087501 (2018).

[45] This is a slight abuse of notation since $1 \leqslant p \leqslant P$ in Eq. (1). However, this may be permitted since there are only p unique time couplings $J_t(p)$ due to the lattice symmetry.

[46] Of course the statistical error in Monte Carlo can be made arbitrarily small given long enough runtime since the sampling error goes as $\mathcal{O}(N_{\mathrm{MC}}^{-1/2})$ for N_{MC} Monte Carlo sweeps. This guarantees that VMC will converge to the free fermion solution in Fig. 5(a) if the globally optimal parameters can be found. The computational time of the MC sampling is $\mathcal{O}(\tau_{\mathrm{corr}} N_{\mathrm{MC}})$ where the autocorrelation time $\tau_{\mathrm{corr}} \sim (PN)^{\gamma}$ is a polynomial function of PN for N spins and P pulses of VITA.

[47] A. W. Sandvik, Ground State Projection of Quantum Spin Systems in the Valence-Bond Basis, Phys. Rev. Lett. **95**, 207203 (2005); Anders W. Sandvik, Stochastic series expansion method for quantum Ising models with arbitrary interactions, Phys. Rev. E **68**, 056701 (2003).